NANO LETTERS

Letter

pubs.acs.org/NanoLett

Self-Collapse Lithography

Chuanzhen Zhao,[†,§] Xiaobin Xu,[†,§] Qing Yang,[†,§] Tianxing Man,[¶] Steven J. Jonas,[▲,■,#] Jeffrey J. Schwartz,[†,△] Anne M. Andrews,[*,†,§,▽] and Paul S. Weiss[*,†,§,□]

[†]California NanoSystems Institute, University of California, Los Angeles, Los Angeles, California 90095, United States

[§]Department of Chemistry and Biochemistry, University of California, Los Angeles, Los Angeles, California 90095, United States

[¶]Department of Mechanical and Aerospace Engineering, University of California, Los Angeles, Los Angeles, California 90095, United States

[▲]Department of Pediatrics, David Geffen School of Medicine, University of California Los Angeles, Los Angeles, California 90095, United States

[■]Eli & Edythe Broad Center of Regenerative Medicine and Stem Cell Research, University of California, Los Angeles, Los Angeles, California 90095, United States

[#]Children's Discovery and Innovation Institute, University of California, Los Angeles, Los Angeles, California 90095, United States

[△]Department of Physics and Astronomy, University of California, Los Angeles, Los Angeles, California 90095, United States

[▽]Department of Psychiatry and Biobehavioral Sciences, Semel Institute for Neuroscience and Human Behavior, and Hatos Center for Neuropharmacology, University of California, Los Angeles, Los Angeles, California 90095, United States

[□]Department of Materials Science and Engineering, University of California, Los Angeles, Los Angeles, California 90095, United States

S *Supporting Information*

ABSTRACT: We report a facile, high-throughput soft lithography process that utilizes nanoscale channels formed naturally at the edges of microscale relief features on soft, elastomeric stamps. Upon contact with self-assembled monolayer (SAM) functionalized substrates, the roof of the stamp collapses, resulting in the selective removal of SAM molecules via a chemical lift-off process. With this technique, which we call self-collapse lithography (SCL), sub-30 nm patterns were achieved readily using masters with microscale features prepared by conventional photolithography. The feature sizes of the chemical patterns can be varied continuously from ∼2 μm to below 30 nm by decreasing stamp relief heights from 1 μm to 50 nm. Likewise, for fixed relief heights, reducing the stamp Young's modulus from ∼2.0 to ∼0.8 MPa resulted in shrinking the features of resulting patterns from ∼400 to ∼100 nm. The self-collapse mechanism was studied using finite element simulation methods to model the competition between adhesion and restoring stresses during patterning. These results correlate well with the experimental data and reveal the relationship between the line widths, channel heights, and Young's moduli of the stamps. In addition, SCL was applied to pattern two-dimensional arrays of circles and squares. These chemical patterns served as resists during etching processes to transfer patterns to the underlying materials (e.g., gold nanostructures). This work provides new insights into the natural propensity of elastomeric stamps to self-collapse and demonstrates a means of exploiting this behavior to achieve patterning via nanoscale chemical lift-off lithography.

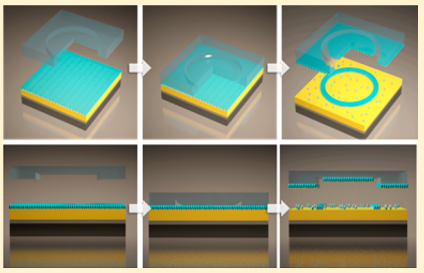

KEYWORDS: *Chemical lift-off lithography, self-collapse, soft lithography, nanolithography*

The rapid development of new and more complex nanoscale technologies, including those in electronics,[1−4] displays and lighting,[5−8] nanofluidics,[9,10] wearable and flexible sensors,[3,11−13] ultrasensitive biosensors,[14−17] and medical devices[18−21] is transforming modern life. To meet demands for further advances in these areas, needs must be met for economical and high-throughput molecular patterning techniques to enable efficient nanofabrication. Conventional photolithography methods cannot achieve robust nanoscale patterns as their resolutions are limited by optical and/or UV light sources and are prohibitively slow for large-area patterning. Additionally, current costs of state-of-the-art nanolithography tools, including parallel approaches (e.g., extreme ultraviolet[22] and X-ray patterning[23]) and direct-write methods (e.g., electron-beam lithography,[24,25] focused ion-beam milling,[26] and scanning probe lithography[27,28]), require highly specialized equipment and significant infrastructural investments that limit availability outside of large corporations and academic and government research centers.

Received: May 30, 2017
Revised: July 17, 2017
Published: July 24, 2017

DOI: 10.1021/acs.nanolett.7b02269
Nano Lett. XXXX, XXX, XXX−XXX

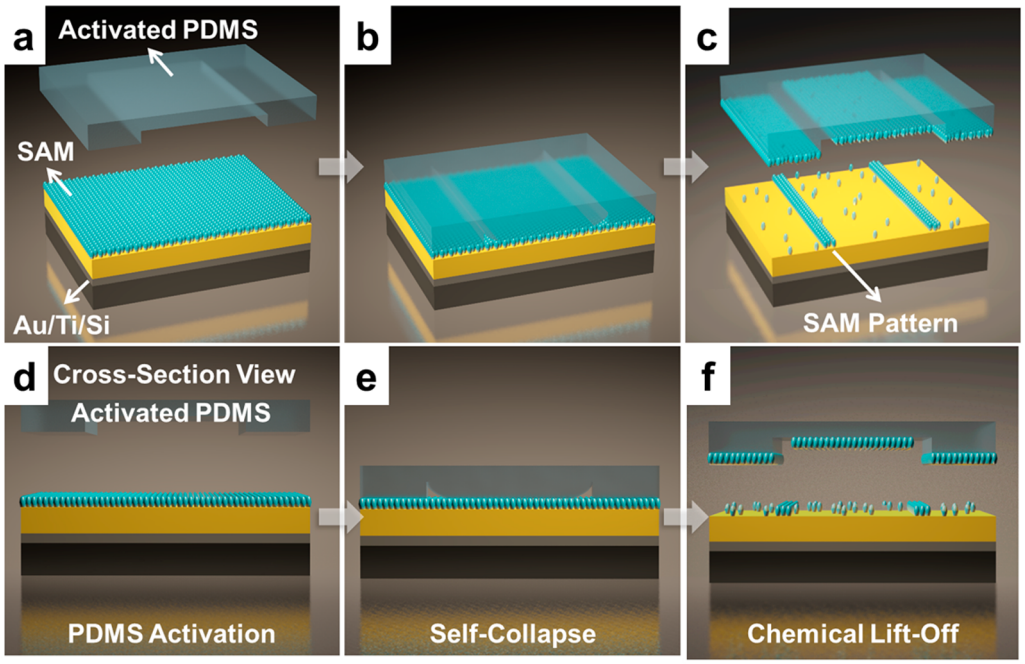

Figure 1. Schematic illustration of self-collapse lithography (SCL). (a,d) Hydroxyl-terminated alkanethiols form a self-assembled monolayer (SAM) on the surface of a Au/Ti-coated Si substrate. A polydimethylsiloxane (PDMS) stamp is activated by oxygen plasma treatment. (b,e) The activated stamp is brought into conformal contact with the SAM-coated Au surface without externally applied forces. (c,f) The chemical lift-off process removes the SAM from regions of the functionalized surface in direct contact with the stamp, thereby producing a pattern from molecules remaining in noncontacted regions.[66]

Several molecular patterning strategies have been developed as economical and accessible alternatives to conventional nanofabrication methods, including soft lithographic microcontact printing (μCP),[29−32] replica molding,[33,34] nanoimprint lithography,[35] polymer pen lithography,[36−40] nanotransfer printing,[41] decal transfer printing,[42] and nanoskiving.[43] The most widely utilized of these methods, μCP, achieves micro- and nanoscale patterning of molecular "inks" (e.g., alkanethiols[29−32] or biomolecules[44−46]) via stamps replica-molded from masters prepared by conventional photolithography. Some molecular inks (e.g., alkanethiols) have been shown to serve as etch resists that enable the transfer of the desired patterns into the underlying substrates.[14,47]

The quality of the final patterns produced via μCP is limited by a variety of factors, including diffusion of molecular inks and/or the deformation of stamp features.[31,32,48] For example, lateral diffusion of ink molecules on surfaces results in enlarged features with lower contrast that can, in some cases, result in the complete loss of the transferred pattern.[31] This effect becomes even more significant when patterning sub-μm features and often limits the resolution of μCP to ∼100 nm. Several modified μCP approaches have been developed by our group to minimize or to eliminate lateral diffusion of ink molecules.[49−52] Microdisplacement printing[50,53] and microcontact insertion printing[31,49,54] were invented to print molecules on alkanethiol self-assembled monolayer (SAM) modified substrates through displacement or insertion processes, respectively. The SAMs in the unpatterned regions prevent ink molecules from diffusing beyond the contact areas.[31,55] We also developed a subtractive molecular patterning method called chemical lift-off lithography (CLL) that effectively eliminates ink-molecule diffusion and is capable of high-fidelity patterning down to 20 nm line widths.[14,52,56] Further refinements of CLL have achieved feature sizes of ∼5 nm.[51]

In addition to lateral diffusion, the accuracy of transferred patterns can also be affected adversely by deformations of stamps upon physical contact with substrates during μCP (e.g., mechanical sagging, sliding, and/or compression of stamp features).[32,57−59] For example, when an external load is applied to a polydimethylsiloxane (PDMS) stamp, the relief features sag causing the roof of the stamp to collapse and to contact the substrate. Recent studies demonstrated that this roof-collapse phenomenon could occur spontaneously even without the application of an external load when the aspect ratio of the stamp features was engineered to be sufficiently large.[57−59] This "self-collapsing" behavior occurs due to the adhesion force between the stamp and substrate. Several groups, including Rogers and coworkers, have investigated stamp designs that minimize self-collapse, which include tailoring feature aspect ratios, adhesion energy, and Young's modulus.[60−63] While seen initially as a disadvantage for pattern reproduction, other groups, including Erickson and colleagues, have harnessed self-collapse for the fabrication of 60 nm nanofluidic channels from microchannels under controlled loads.[64,65] We have also exploited this phenomenon for precise control of patterns using polymer-pen arrays and integral supporting structures.[40] However, to the best of our knowledge, self-collapse has not been specifically exploited for nanolithography.

Here, we report control of self-collapse behavior of PDMS stamps precisely at the nanoscale when integrated with CLL to establish a new nanolithography method: self-collapse lithography (SCL). Using SCL, we achieve sub-30 nm features by tailoring the dimensions of the stamp features, as well as the stiffness of the PDMS.

A typical SCL process is illustrated in Figure 1 where, in Step 1, a Au (30 nm)/Ti (10 nm)/Si substrate is immersed into a

DOI: 10.1021/acs.nanolett.7b02269
Nano Lett. XXXX, XXX, XXX−XXX

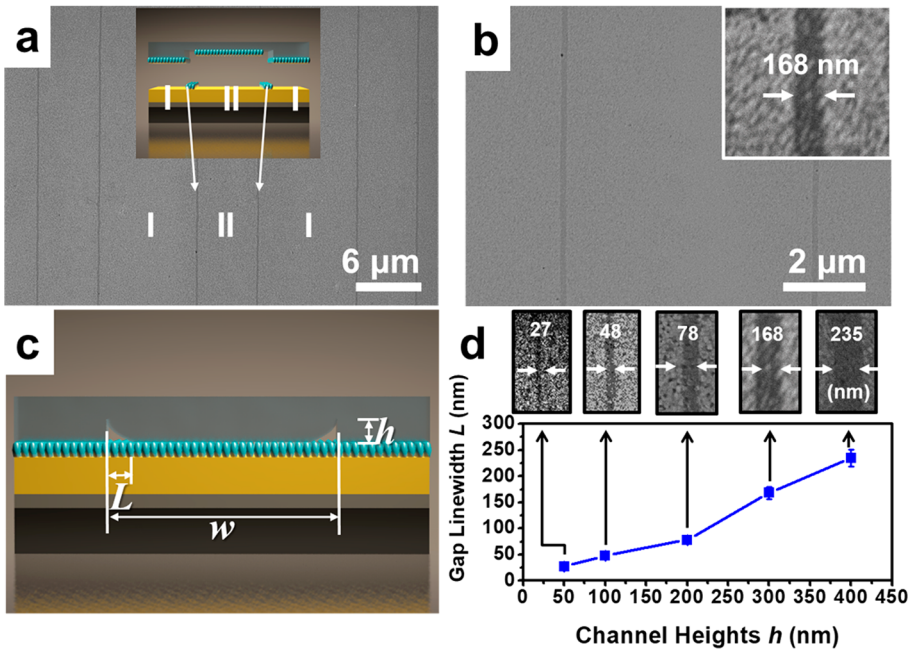

Figure 2. (a,b) Scanning electron microscope (SEM) images of linear arrays with sub-200 nm line widths created by self-collapse lithography using a stamp with microchannel features (6 μm channel width, 300 nm channel height). (c) Schematic illustration of a collapsed stamp (L, gap line width; w, channel width; and h, channel height). (d) Plot of gap line widths L obtained using different channel heights h with a fixed Young's modulus of 1.75 MPa. The channel width for each data point is listed in Table 1. Insets correspond to a representative SEM image for each data point.

hydroxyl-terminated alkanethiol solution (1 mM 11-mercapto-1-undecanol in ethanol) for ~12 h to form a SAM on the Au surface. Next, a PDMS stamp with the desired pattern is "activated" by exposure to oxygen plasma for 40 s, which generates hydrophilic silanol (—Si—OH) groups on the stamp surface. In Step 2, an activated stamp is placed in conformal contact with the SAM-functionalized Au surface without an externally applied load. The Au surface is flame annealed before functionalization. The surface roughness is ~1 nm, which is necessary for the subsequent high-resolution chemical patterning. Self-collapse of the stamp's recessed features occurs spontaneously due to adhesion forces between the PDMS and the SAM on the Au surface. Covalent bonds form via condensation reactions between the −OH moieties of the SAM and the silanol groups of the activated PDMS stamp in direct contact with the surface (i.e., the self-collapsing regions and the protruding features).[47] Upon lifting the PDMS stamp off the substrate (Step 3), alkanethiol molecules are removed selectively from the Au surface in the stamp-contact regions, leaving intact SAMs in the noncontacted areas. As observed in CLL, Au atoms are also removed during lift-off as the Au−S bonds between alkanethiol adsorbates and Au surface atoms are stronger than Au−Au bonds at the surface of the substrate.[51,52] Note that as discovered in our previous work and shown in Figure 1c,f, not all of the molecules in the contact regions are removed in the CCL process (and the remaining molecules can form a matrix for controlled chemical patterning).[40,66]

For self-collapse to occur, the aspect ratios (channel width/height) of stamp features and Young's modulus must satisfy specific criteria.[60] We assembled stamps with recessed channels having widths and heights configured to collapse at desired locations, resulting in controlled, reproducible patterns. Scanning electron microscope (SEM) images, as seen in Figure 2, demonstrate the removal of SAMs in regions that were in conformal contact with the stamps. Due to stamp self-collapse, narrow structures with line widths much smaller than the original channel dimensions were observed on the SCL-patterned surface. In Figure 2a,b, arrays of lines ~170 nm wide were produced via SCL using PDMS stamps with 6 μm wide channels and 300 nm channel heights. The patterned lines were straight and continuous for tens of micrometers, corresponding to the edges of the original microscale channel. Despite one side of the line being determined by the edge of the stamp contact and the other side being determined by the collapsed polymer, no significant differences in the two sides of the patterned features were observed in these and other patterns.

We identified a set of basic design rules that govern SCL to understand the effects of key parameters on the final patterns. It has previously been reported that for reproducible self-collapse to occur, the channel width needs to be larger than a threshold value fixed for each value of the Young's modulus of the stamps, where the potential energy for the collapse is employed to determine the threshold.[60] The aspect ratios (channel width/height) of the stamp features were engineered to be sufficiently large to enable self-collapse.[60] We denote stamp features as follows: channel width as w, channel height as h, and the noncollapsed gap line width as L (Figure 2c). We first examined the dependence of L on h. Stamps with discrete values of h, within the range of 50 (w = 1 μm) to 400 nm (w = 10 μm), produced patterned lines with L values of 27 ± 5, 48 ± 6, 78 ± 6, 168 ± 12, and 235 ± 17 nm, respectively, as shown in Figure 2d and reported in Table 1. The channel width for each height is highlighted in the table. Note that when w is larger than this threshold value, at fixed h, changes in w have little influence on L,[60] in agreement with our experimental results. For example, we obtained similar values of L at 235 or 227 nm for different values w at 10 or 20 μm, respectively, with h fixed at 400 nm.[60,62] We kept the thickness of PDMS stamps the same (5 mm) in all experiments, and the influence of gravity was neglected in this study. Note that the applied

DOI: 10.1021/acs.nanolett.7b02269
Nano Lett. XXXX, XXX, XXX−XXX

Table 1. Gap Line Widths (L) Produced Using Stamps with Different Channel Heights (h) and Channel Widths (w), with a Fixed Young's Modulus (E = 1.75 MPa)

h (nm)	L (nm)	w (μm)
50	27 ± 5	1
100	48 ± 6	4
200	78 ± 6	6
300	168 ± 12	6
400	235 ± 17	10
400	227 ± 19	20
500	411 ± 9	20
700	872 ± 82	20
1000	1710 ± 98	80

external force and the thickness of the PDMS could also be used to control L, e.g., smaller widths can be achieved by applying external stress, which is currently under investigation.

Next, we investigated the relationship between L and the Young's modulus (E) of stamps. The PDMS stamps were prepared using different ratios (X/Y) of Sylgard 184 prepolymer base (X) and curing agent (Y) to control the relationship with the patterned line widths. Values of E were estimated based on previous reports with details included in the Supporting Information.[67−69] Stamps with E ranging from 0.85 to 2.0 MPa were molded from a master with relief channel heights fixed at 400 nm. When these stamps were utilized for SCL, L was found to decrease proportionally with decreasing E (Table 2). These results indicate that SCL patterns can be fine-tuned by varying stamp stiffness, i.e., a smaller L can be achieved by using softer stamps.

Table 2. Gap Line Widths (L) Produced Using Stamps with Different Young's Moduli (E), and a Fixed Channel Height (h = 400 nm) and Width (w = 10 μm)

E (MPa)	L (nm)
2.0	366 ± 12
1.15	165 ± 16
1.75	235 ± 17
0.85	100 ± 17

A key distinction between SCL and other soft lithographic strategies is that nanoscale patterns are generated from the deformation of micron-scale features on stamps molded from conventional photolithographically prepared masters. The self-collapse process transfers the two-dimensional (2D) pattern of the stamp features to the surface while avoiding scaling issues that limit conventional lithographic methods. In principle, the scale over which stamp patterns are reduced is limited only by the precision to which masters can be fabricated and the degree of control over stamp stiffness.

Adhesion forces between the stamp and the underlying substrate drive the self-collapse of recessed elastomer features. Previously, this process has been approximated using a classic crack growth model (i.e., crack growth stops when the required work equals the adhesion energy) by Huang et al.[60,62] Here, we examined the self-collapse process more directly by modeling stress distributions along the gap (L) between collapsed regions and the edges of the original features. Two stresses compete at the edges of the gap: an elastic restoring force (σ_r) and an adhesion force (σ_a), both acting normal to the substrate. Interactions between σ_r and σ_a can be used to predict L during SCL (Figure 3a). The adhesion force acts to collapse the top of the channel, pulling it toward the substrate surface, while the restoring force acts to retain the shape of the channel, pulling it away from the substrate. At equilibrium ($\sigma_r = \sigma_a$), a stable gap (L) is formed between the collapsed top and edges of the channel.

Finite element analysis (FEA) simulations were carried out using the ANSYS software suite (Ansys Inc. Student version 16.0, Canonsburg, PA) to model the distributions of mechanical stress within a stamp with minimum mesh sizes fixed at 100 nm (Figure 3b). We employed an inverse method to simulate the mechanism of self-collapse, where the roofs of simulated channels of specified widths were displaced toward their corresponding substrates by an amount equal to the channel height, h. By varying the width of the simulated channel roof, we obtained a series of restoring stresses along the gap edges and their corresponding gap line widths, L. In this way, we simulated the collapse of stamps configured with different channel heights to obtain an approximate relationship between the restoring stress and gap width at different channel heights.

As illustrated in Figure 3c, increases in stamp channel heights result in increases in the resulting gap line widths as less of each channel's roof makes contact with the substrate surface at fixed stress. A comparison of the results from our FEA simulations at adhesion stresses of 2.0 and 2.1 MPa with those obtained from SCL experiments are shown in Figure 3d. There is excellent agreement between simulated responses and experimental data, indicating that our stress-balance model correlates well and is predictive of the self-collapse phenomenon. Moreover, the simulation results can be used to predict the line widths of patterns with smaller features. Fitting a parabolic function to the 2.0 MPa curve (Figure 3e):

$$L = f(h) = ah + bh^2 \quad (1)$$

We determined the fitting constants a = 0.038 nm^{-1} and b = 0.00156 nm^{-2}. Using eq 1, we can estimate the L of a pattern produced with any h at stable collapse regions, which enables the manipulation of SCL-generated patterns via strategic design of stamp features. For example, to achieve a line width of 100 nm, a stamp with channel height of $h \approx 242$ nm is needed, according to eq 1. With proper design and optimization, we estimate that SCL will be able to produce line widths as small as 5 nm (corresponding to patterns about 10 molecules across).[40,51]

In addition to channel height, our studies demonstrate how the mechanical stiffness of PDMS affects line widths of the final pattern. We modeled the behavior of stamps using different ratios of Sylgard 184 prepolymer base to curing agent to determine the relationship with the pattern line width. Simulation results of stress and L, at a fixed channel height of 400 nm, are shown in Figure S1 using different values of E: 2.0 MPa (5:1), 1.75 MPa (10:1), 1.15 MPa (15:1), and 0.85 MPa (20:1). Analyses of these data were used to visualize the relationship between E and L (Figure 3f). A trend emerges showing that a decrease in E (i.e., as the PDMS stamp becomes softer) results in smaller values of L when patterning using stamps with identical channel heights. Therefore, stamps derived from a single master may be used to generate a range of feature sizes by varying E.

To demonstrate the versatility of SCL, we produced a variety of patterns, including arrays of circle and square features from PDMS stamps comprising micron-scale, recessed circular or

DOI: 10.1021/acs.nanolett.7b02269
Nano Lett. XXXX, XXX, XXX−XXX

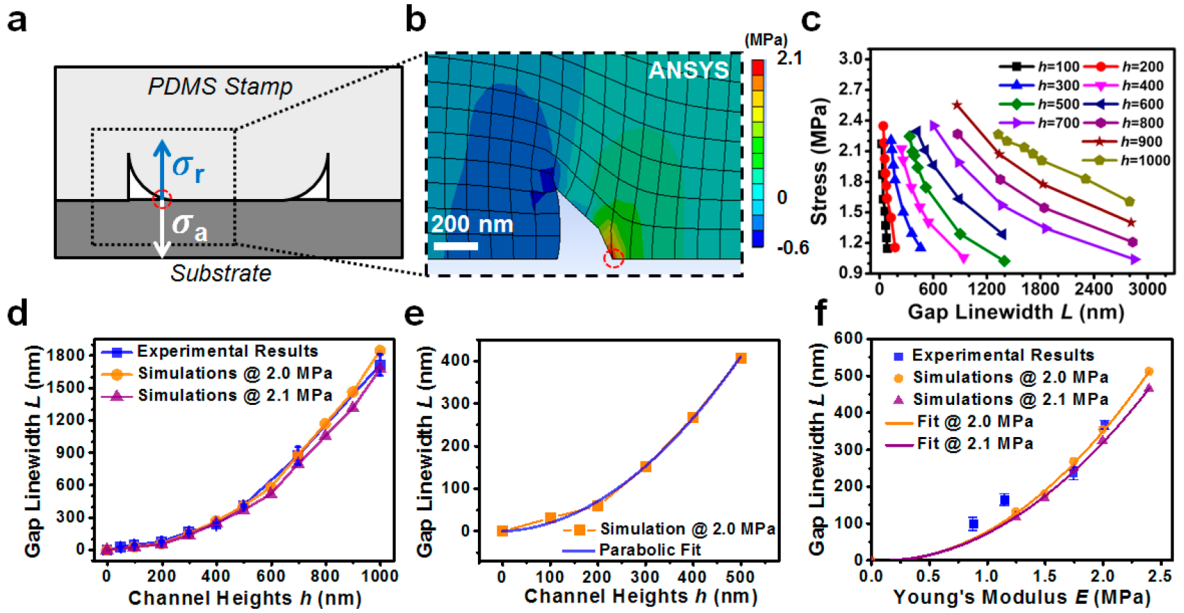

Figure 3. (a) Schematic illustration of the self-collapse model used in finite element analysis (FEA) simulations, where σ_r represents the restoring stress and σ_a denotes the adhesion stress between the PDMS stamp and the substrate. (b) A typical FEA simulation result illustrating the stress distribution on a self-collapse stamp (only the restoring stresses normal to the substrate are depicted). (c) Relationships between simulated stresses and gap sizes L at different channel heights h. (d) Experimentally measured gap widths and channel heights (squares) plotted with simulated values (circles, triangles) using Young's moduli (E) of 2.0 and 2.1 MPa. (e) Simulated gap line widths plotted as a function of channel height with a parabolic fit. (f) Plots of simulated and experimental results showing variations in gap line widths at different values of E.

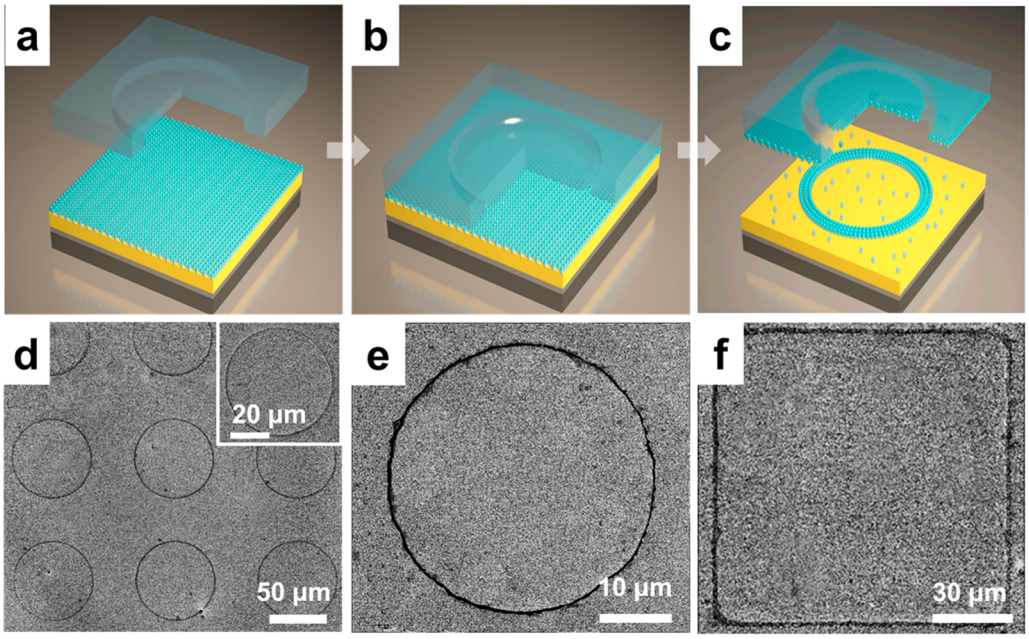

Figure 4. (a–c) Schematic illustrations of a ring chemical pattern fabricated via SCL. (a) Hydroxyl-terminated alkanethiols form a self-assembled monolayer (SAM) on the surface of an Au/Ti-coated Si substrate. (b) A stamp with recessed circular features is activated by oxygen plasma and then placed into conformal contact with the functionalized Au surface, without an external force. The central portions of the recessed features on the stamp contact the underlying SAM in smaller circular regions due to self-collapse. (c) The chemical lift-off process removes the SAM in direct contact with the polydimethlysiloxane (PDMS) surfaces from the Au substrate, leaving raised (dark), ring-like SAM patterns behind. (d–f) Contrast enhanced SEM images of (d) ring patterns ($L \approx 1.71$ μm), patterned by SCL with a stamp with recessed circles (50 μm in diameter and 1 μm in height), (e) a ring pattern ($L \approx 235$ nm) patterned using recessed circles (40 μm in diameter and 400 nm in height), and (f) raised (dark) squares ($L \approx 1.71$ μm) patterned with recessed square structures (100 μm on each edge and 1 μm in height).

square features, as illustrated in Figures 4 and 5. Nanoscale patterning of other shapes can be similarly achieved by careful design of the stamp mold. To date, we have produced robust arrays of ~250 nm line width circular rings via SCL from stamps comprising circular holes with diameters of ~40 μm and heights of ~400 nm (Figure 4e). By deconstructing these patterns into component lines and angular elements, it is possible to extend SCL further to achieve more complex

DOI: 10.1021/acs.nanolett.7b02269
Nano Lett. XXXX, XXX, XXX−XXX

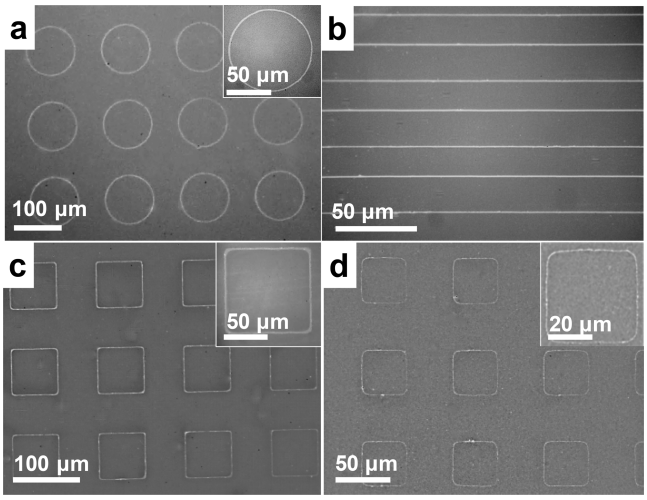

Figure 5. Optical microscope images of Au micro-/nanostructures fabricated by self-collapse lithography (SCL) followed by selective etching. (a) The Au rings with line widths of 1.71 μm were fabricated using stamps patterned with 100 μm diameter circles recessed by 1 μm. (b) Here, Au lines 870 nm wide were fabricated using stamps possessing recessed linear features that were 40 μm wide and 700 nm deep. (c) Sub-2 μm Au squares fabricated using stamps patterned with recessed square features that were 100 μm on an edge and 1 μm in height. (d) Sub-250 nm Au squares fabricated using stamps with recessed squares that were 40 μm in width and 400 nm in height.

pattern configurations, such as those needed for circuits for nanoelectronics.

The chemical patterns produced via SCL can be utilized as templates for selectively patterning a variety of materials, including metals and biomolecules. For example, the intact SAM that remains on a Au substrate following SCL can resist selective chemical etching, enabling the creation of Au nanostructures, including large-area arrays of Au micro-/nano-rings, wires, or square structures (Figure 5). We used atomic force microscopy for depth analysis to image the SAM patterns by CLL and, in our previous work, wet etching processed samples.[52] Nanostructures of other materials such as silver and copper can be fabricated similarly. As demonstrated by our prior work in developing CLL, SCL may also be applied to pattern biomolecules at the nanoscale.[40,51,52,56,70]

In summary, SCL represents a facile and robust nanolithography technique to achieve sub-30 nm resolution by exploiting the elasticity of PDMS structures and natural stamp−substrate adhesion forces. A wide range of shapes and feature sizes can be patterned by strategically designing stamp feature dimensions (e.g., height/width) and/or Young's modulus. Importantly, this soft-lithographic approach can be used as a complement or alternative to slow and expensive direct-writing processes (e.g., electron-beam lithography). The SCL technique provides new insight into how a previously undesirable characteristic of soft lithography can be exploited, via CLL, to yield nanoscale patterns. Finite element model simulations suggest a straightforward mechanism for the self-collapse process through the competition between restoring and adhesion stresses along the gap edge produced between the protruding and collapsed stamp features. Results from these simulations correlate well with experimental data and elucidate design rules for using controlled self-collapse to generate complex patterns at the nanoscale that can be applied broadly to applications in nanoelectronics, biosensing, energy storage, and catalysis.

■ ASSOCIATED CONTENT

Supporting Information

The Supporting Information is available free of charge on the ACS Publications website at DOI: 10.1021/acs.nanolett.7b02269.

Experimental details describing the fabrication of Si masters and PDMS stamps, characterization of chemical patterns and stamps, surface functionalization of Au/Ti/Si substrates, activation of PDMS stamps, and Au wet-etching process; estimation process of Young's moduli of PDMS; raw scanning electron micrograph depicted in Figure 4d−f; and plot of simulation results using different Young's moduli (PDF)

■ AUTHOR INFORMATION

Corresponding Authors

*E-mail: aandrews@mednet.ucla.edu.
*E-mail: psw@cnsi.ucla.edu.

ORCID

Chuanzhen Zhao: 0000-0003-0162-1231
Xiaobin Xu: 0000-0002-3479-0130
Qing Yang: 0000-0003-4422-5300
Tianxing Man: 0000-0001-5079-3844
Steven J. Jonas: 0000-0002-8111-0249
Jeffrey J. Schwartz: 0000-0003-1544-1901
Anne M. Andrews: 0000-0002-1961-4833
Paul S. Weiss: 0000-0001-5527-6248

Author Contributions

The experiments were designed by C.Z., X.X., and P.S.W. Data were collected by C.Z., X.X., Q.Y., and T.M. and were analyzed by C.Z., X.X., P.S.W., and A.M.A. Figures were prepared by C.Z., X.X., and J.J.S. The manuscript was written by C.Z., X.X., S.J.J., J.J.S., P.S.W., and A.M.A. with assistance from all other authors.

Notes

The authors declare no competing financial interest.

■ ACKNOWLEDGMENTS

This work was supported by National Science Foundation Grant #CMMI-1636136. C.Z. and T.M. thank the China Scholarship Council for CSC-UCLA scholarship. S.J.J. and P.S.W. acknowledge the support of the Eli and Edythe Broad Center of Regenerative Medicine and Stem Cell Research at UCLA Training Program through its Clinical Fellowship Training Award Program as well as the UCLA Children's Discovery and Innovation Institute's (CDI) Fellows Research Support Award. We also acknowledge the facilities and thank the staff of the Nanoelectronics Research Facility (NRF), Electron Imaging Center, Nano & Pico Characterization Lab, and Integrated Systems Nanofabrication Cleanroom of the California NanoSystems Institute, especially Tom Lee, Krissy Do, and Lorna Tokunaga.

■ REFERENCES

(1) Yan, H.; Chen, Z.; Zheng, Y.; Newman, C.; Quinn, J. R.; Dotz, F.; Kastler, M.; Facchetti, A. *Nature* **2009**, *457*, 679−686.
(2) Jeon, H.-J.; Kim, K. H.; Baek, Y.-K.; Kim, D. W.; Jung, H.-T. *Nano Lett.* **2010**, *10*, 3604−3610.

DOI: 10.1021/acs.nanolett.7b02269
Nano Lett. XXXX, XXX, XXX−XXX

(3) Kim, D.-H.; Lu, N.; Ma, R.; Kim, Y.-S.; Kim, R.-H.; Wang, S.; Wu, J.; Won, S. M.; Tao, H.; Islam, A.; Yu, K. J.; Kim, T.-I.; Chowdhury, R.; Ying, M.; Xu, L.; Li, M.; Chung, H.-J.; Keum, H.; Mccormick, M.; Liu, P.; Zhang, Y.-W.; Omenetto, F. G.; Huang, Y.; Coleman, T.; Rogers, J. A. *Science* **2011**, *333*, 838−843.
(4) Tsai, H.; Pitera, J. W.; Miyazoe, H.; Bangsaruntip, S.; Engelmann, S. U.; Liu, C.-C.; Cheng, J. Y.; Bucchignano, J. J.; Klaus, D. P.; Joseph, E. A.; Sanders, D. P.; Colburn, M. E.; Guillorn, M. A. *ACS Nano* **2014**, *8*, 5227−5232.
(5) Kim, T.-H.; Cho, K.-S.; Lee, E. K.; Lee, S. J.; Chae, J.; Kim, J. W.; Kim, D. H.; Kwon, J.-Y.; Amaratunga, G.; Lee, S. Y.; Choi, B. L.; Kuk, Y.; Kim, J. M.; Kim, K. *Nat. Photonics* **2011**, *5*, 176−182.
(6) Kim, B. H.; Onses, M. S.; Lim, J. B.; Nam, S.; Oh, N.; Kim, H.; Yu, K. J.; Lee, J. W.; Kim, J.-H.; Kang, S.-K.; Lee, C. H.; Lee, J.; Shin, J. H.; Kim, N. H.; Leal, C.; Shim, M.; Rogers, J. A. *Nano Lett.* **2015**, *15*, 969−973.
(7) Kim, B. H.; Nam, S.; Oh, N.; Cho, S.-Y.; Yu, K. J.; Lee, C. H.; Zhang, J.; Deshpande, K.; Trefonas, P.; Kim, J.-H.; Lee, J.; Shin, J. H.; Yu, Y.; Lim, J. B.; Won, S. M.; Cho, Y. K.; Kim, N. H.; Seo, K. J.; Lee, H.; Kim, T.-I.; Shim, M.; Rogers, J. A. *ACS Nano* **2016**, *10*, 4920−4925.
(8) Park, J.-S.; Kyhm, J.; Kim, H. H.; Jeong, S.; Kang, J.; Lee, S.-E.; Lee, K.-T.; Park, K.; Barange, N.; Han, J.; Song, J. D.; Choi, W. K.; Han, I. K. *Nano Lett.* **2016**, *16*, 6946−6953.
(9) Whitesides, G. M. *Nature* **2006**, *442*, 368−373.
(10) Liang, X.; Morton, K. J.; Austin, R. H.; Chou, S. Y. *Nano Lett.* **2007**, *7*, 3774−3780.
(11) Rogers, J. A.; Someya, T.; Huang, Y. *Science* **2010**, *327*, 1603−1607.
(12) Gao, W.; Emaminejad, S.; Nyein, H. Y. Y.; Challa, S.; Chen, K.; Peck, A.; Fahad, H. M.; Ota, H.; Shiraki, H.; Kiriya, D.; Lien, D.-H.; Brooks, G. A.; Davis, R. W.; Javey, A. *Nature* **2016**, *529*, 509−514.
(13) Xu, J.; Wang, S.; Wang, G.-J. N.; Zhu, C.; Luo, S.; Jin, L.; Gu, X.; Chen, S.; Feig, V. R.; To, J. W. F.; Rondeau-Gagné, S.; Park, J.; Schroeder, B. C.; Lu, C.; Oh, J. Y.; Wang, Y.; Kim, Y.-H.; Yan, H.; Sinclair, R.; Zhou, D.; Xue, G.; Murmann, B.; Linder, C.; Cai, W.; Tok, J. B. H.; Chung, J. W.; Bao, Z. *Science* **2017**, *355*, 59−64.
(14) Kim, J.; Rim, Y. S.; Chen, H.; Cao, H. H.; Nakatsuka, N.; Hinton, H. L.; Zhao, C.; Andrews, A. M.; Yang, Y.; Weiss, P. S. *ACS Nano* **2015**, *9*, 4572−4582.
(15) Rim, Y. S.; Bae, S.-H.; Chen, H.; Yang, J. L.; Kim, J.; Andrews, A. M.; Weiss, P. S.; Yang, Y.; Tseng, H.-R. *ACS Nano* **2015**, *9*, 12174−12181.
(16) Limaj, O.; Etezadi, D.; Wittenberg, N. J.; Rodrigo, D.; Yoo, D.; Oh, S.-H.; Altug, H. *Nano Lett.* **2016**, *16*, 1502−1508.
(17) Liu, Q.; Aroonyadet, N.; Song, Y.; Wang, X.; Cao, X.; Liu, Y.; Cong, S.; Wu, F.; Thompson, M. E.; Zhou, C. *ACS Nano* **2016**, *10*, 10117−10125.
(18) Hochbaum, A. I.; Aizenberg, J. *Nano Lett.* **2010**, *10*, 3717−3721.
(19) Ul-Haq, E.; Patole, S.; Moxey, M.; Amstad, E.; Vasilev, C.; Hunter, C. N.; Leggett, G. J.; Spencer, N. D.; Williams, N. H. *ACS Nano* **2013**, *7*, 7610−7618.
(20) Chiappini, C.; De Rosa, E.; Martinez, J. O.; Liu, X.; Steele, J.; Stevens, M. M.; Tasciotti, E. *Nat. Mater.* **2015**, *14*, 532−539.
(21) Moxey, M.; Johnson, A.; El-Zubir, O.; Cartron, M.; Dinachali, S. S.; Hunter, C. N.; Saifullah, M. S. M.; Chong, K. S. L.; Leggett, G. J. *ACS Nano* **2015**, *9*, 6262−6270.
(22) Wagner, C.; Harned, N. *Nat. Photonics* **2010**, *4*, 24−26.
(23) Miszta, K.; Greullet, F.; Marras, S.; Prato, M.; Toma, A.; Arciniegas, M.; Manna, L.; Krahne, R. *Nano Lett.* **2014**, *14*, 2116−2122.
(24) Manfrinato, V. R.; Wen, J.; Zhang, L.; Yang, Y.; Hobbs, R. G.; Baker, B.; Su, D.; Zakharov, D.; Zaluzec, N. J.; Miller, D. J.; Stach, E. A.; Berggren, K. K. *Nano Lett.* **2014**, *14*, 4406−4412.
(25) Bat, E.; Lee, J.; Lau, U. Y.; Maynard, H. D. *Nat. Commun.* **2015**, *6*, 6654.
(26) Volkert, C. A.; Minor, A. M. *MRS Bull.* **2007**, *32*, 389−399.
(27) Xu, S.; Liu, G. Y. *Langmuir* **1997**, *13*, 127−129.
(28) Piner, R. D.; Zhu, J.; Xu, F.; Hong, S. H.; Mirkin, C. A. *Science* **1999**, *283*, 661−663.
(29) Kumar, A.; Whitesides, G. M. *Appl. Phys. Lett.* **1993**, *63*, 2002−2004.
(30) Xia, Y.; Whitesides, G. M. *Angew. Chem., Int. Ed.* **1998**, *37*, 550−575.
(31) Srinivasan, C.; Mullen, T. J.; Hohman, J. N.; Anderson, M. E.; Dameron, A. A.; Andrews, A. M.; Dickey, E. C.; Horn, M. W.; Weiss, P. S. *ACS Nano* **2007**, *1*, 191−201.
(32) Qin, D.; Xia, Y.; Whitesides, G. M. *Nat. Protoc.* **2010**, *5*, 491−502.
(33) Xia, Y. N.; Mcclelland, J. J.; Gupta, R.; Qin, D.; Zhao, X. M.; Sohn, L. L.; Celotta, R. J.; Whitesides, G. M. *Adv. Mater.* **1997**, *9*, 147−149.
(34) Tian, C.; Kim, H.; Sun, W.; Kim, Y.; Yin, P.; Liu, H. *ACS Nano* **2017**, *11*, 227−238.
(35) Chou, S. Y.; Krauss, P. R.; Renstrom, P. J. *Science* **1996**, *272*, 85−87.
(36) Huo, F.; Zheng, Z.; Zheng, G.; Giam, L. R.; Zhang, H.; Mirkin, C. A. *Science* **2008**, *321*, 1658−1660.
(37) Shim, W.; Braunschweig, A. B.; Liao, X.; Chai, J.; Lim, J. K.; Zheng, G.; Mirkin, C. A. *Nature* **2011**, *469*, 516−520.
(38) Zhong, X.; Bailey, N. A.; Schesing, K. B.; Bian, S.; Campos, L. M.; Braunschweig, A. B. *J. Polym. Sci., Part A: Polym. Chem.* **2013**, *51*, 1533−1539.
(39) Liao, X.; Huang, Y.-K.; Mirkin, C. A.; Dravid, V. P. *ACS Nano* **2017**, *11*, 4439.
(40) Xu, X.; Yang, Q.; Cheung, K. M.; Zhao, C.; Wattanatorn, N.; Belling, J. N.; Abendroth, J. M.; Slaughter, L. S.; Mirkin, C. A.; Andrews, A. M.; Weiss, P. S. *Nano Lett.* **2017**, *17*, 3302−3311.
(41) Jeon, S.; Menard, E.; Park, J. U.; Maria, J.; Meitl, M.; Zaumseil, J.; Rogers, J. A. *Adv. Mater.* **2004**, *16*, 1369−1373.
(42) Childs, W. R.; Nuzzo, R. G. *J. Am. Chem. Soc.* **2002**, *124*, 13583−13596.
(43) Xu, Q. B.; Rioux, R. M.; Dickey, M. D.; Whitesides, G. M. *Acc. Chem. Res.* **2008**, *41*, 1566−1577.
(44) James, C. D.; Davis, R. C.; Kam, L.; Craighead, H. G.; Isaacson, M.; Turner, J. N.; Shain, W. *Langmuir* **1998**, *14*, 741−744.
(45) Bernard, A.; Renault, J. P.; Michel, B.; Bosshard, H. R.; Delamarche, E. *Adv. Mater.* **2000**, *12*, 1067−1070.
(46) Vaish, A.; Shuster, M. J.; Cheunkar, S.; Weiss, P. S.; Andrews, A. M. *Small* **2011**, *7*, 1471−1479.
(47) Xia, Y.; Zhao, X.-M.; Kim, E.; Whitesides, G. M. *Chem. Mater.* **1995**, *7*, 2332−2337.
(48) Delamarche, E.; Schmid, H.; Bietsch, A.; Larsen, N. B.; Rothuizen, H.; Michel, B.; Biebuyck, H. *J. Phys. Chem. B* **1998**, *102*, 3324−3334.
(49) Mullen, T. J.; Srinivasan, C.; Hohman, J. N.; Gillmor, S. D.; Shuster, M. J.; Horn, M. W.; Andrews, A. M.; Weiss, P. S. *Appl. Phys. Lett.* **2007**, *90*, 063114.
(50) Dameron, A. A.; Hampton, J. R.; Smith, R. K.; Mullen, T. J.; Gillmor, S. D.; Weiss, P. S. *Nano Lett.* **2005**, *5*, 1834−1837.
(51) Andrews, A. M.; Liao, W.-S.; Weiss, P. S. *Acc. Chem. Res.* **2016**, *49*, 1449−1457.
(52) Liao, W.-S.; Cheunkar, S.; Cao, H. H.; Bednar, H. R.; Weiss, P. S.; Andrews, A. M. *Science* **2012**, *337*, 1517−1521.
(53) Saavedra, H. M.; Mullen, T. J.; Zhang, P. P.; Dewey, D. C.; Claridge, S. A.; Weiss, P. S. *Rep. Prog. Phys.* **2010**, *73*, 036501.
(54) Shuster, M. J.; Vaish, A.; Cao, H. H.; Guttentag, A. I.; Mcmanigle, J. E.; Gibb, A. L.; Martinez, M. M.; Nezarati, R. M.; Hinds, J. M.; Liao, W. S.; Weiss, P. S.; Andrews, A. M. *Chem. Commun.* **2011**, *47*, 10641−10643.
(55) Claridge, S. A.; Liao, W. S.; Thomas, J. C.; Zhao, Y.; Cao, H. H.; Cheunkar, S.; Serino, A. C.; Andrews, A. M.; Weiss, P. S. *Chem. Soc. Rev.* **2013**, *42*, 2725−2745.
(56) Cao, H. H.; Nakatsuka, N.; Serino, A. C.; Liao, W.-S.; Cheunkar, S.; Yang, H.; Weiss, P. S.; Andrews, A. M. *ACS Nano* **2015**, *9*, 11439−11454.

DOI: 10.1021/acs.nanolett.7b02269
Nano Lett. XXXX, XXX, XXX−XXX

(57) Hui, C. Y.; Jagota, A.; Lin, Y. Y.; Kramer, E. J. *Langmuir* **2002**, *18*, 1394−1407.
(58) Sharp, K. G.; Blackman, G. S.; Glassmaker, N. J.; Jagota, A.; Hui, C. Y. *Langmuir* **2004**, *20*, 6430−6438.
(59) Hsia, K. J.; Huang, Y.; Menard, E.; Park, J. U.; Zhou, W.; Rogers, J.; Fulton, J. M. *Appl. Phys. Lett.* **2005**, *86*, 154106.
(60) Huang, Y. G. Y.; Zhou, W. X.; Hsia, K. J.; Menard, E.; Park, J. U.; Rogers, J. A.; Alleyne, A. G. *Langmuir* **2005**, *21*, 8058−8068.
(61) Zhou, W.; Huang, Y.; Menard, E.; Aluru, N. R.; Rogers, J. A.; Alleyne, A. G. *Appl. Phys. Lett.* **2005**, *87*, 251925.
(62) Xue, Y.; Zhang, Y.; Feng, X.; Kim, S.; Rogers, J. A.; Huang, Y. *J. Mech. Phys. Solids* **2015**, *77*, 27−42.
(63) Xue, Y.; Kang, D.; Ma, Y.; Feng, X.; Rogers, J. A.; Huang, Y. *Extreme Mech. Lett.* **2017**, *11*, 18−23.
(64) Huh, D.; Mills, K. L.; Zhu, X.; Burns, M. A.; Thouless, M. D.; Takayama, S. *Nat. Mater.* **2007**, *6*, 424−428.
(65) Park, S. M.; Huh, Y. S.; Craighead, H. G.; Erickson, D. *Proc. Natl. Acad. Sci. U. S. A.* **2009**, *106*, 15549−15554.
(66) Cao, H. H.; Nakatsuka, N.; Serino, A. C.; Liao, W. S.; Cheunkar, S.; Yang, H.; Weiss, P. S.; Andrews, A. M. *ACS Nano* **2015**, *9*, 11439−11454.
(67) Armani, D.; Liu, C.; Aluru, N. *Proc. IEEE MEMS99* **1999**, 222−227.
(68) Carrillo, F.; Gupta, S.; Balooch, M.; Marshall, S. J.; Marshall, G. W.; Pruitt, L.; Puttlitz, C. M. *J. Mater. Res.* **2005**, *20*, 2820−2830.
(69) Johnston, I. D.; McCluskey, D. K.; Tan, C. K. L.; Tracey, M. C. *J. Micromech. Microeng.* **2014**, *24*, 035017.
(70) Cao, H. H.; Nakatsuka, N.; Liao, W.-S.; Serino, A. C.; Cheunkar, S.; Yang, H.; Weiss, P. S.; Andrews, A. M. *Chem. Mater.* **2017**, DOI: 10.1021/acs.chemmater.7b01970.

DOI: 10.1021/acs.nanolett.7b02269
Nano Lett. XXXX, XXX, XXX−XXX